Surface Micromachined Capacitive Ultrasonic Transducers

Igal Ladabaum, *Student Member, IEEE*, Xuecheng Jin, *Student Member, IEEE*,
Hyongsok T. Soh, Abdullah Atalar, *Senior Member, IEEE*,
and Butrus T. Khuri-Yakub, *Fellow, IEEE*

***Abstract*—The current state of a novel technology, surface microfabricated ultrasonic transducers, is reported. Experiments demonstrating both air and water transmission are presented. Air-coupled longitudinal wave transmission through aluminum is demonstrated, implying a 110 dB dynamic range for transducers at 2.3 MHz in air. Water transmission experiments from 1 to 20 MHz are performed, with a measured 60 dB SNR at 3 MHz. A theoretical model is proposed that agrees well with observed transducer behavior. Most significantly, the model is used to demonstrate that microfabricated ultrasonic transducers constitute an attractive alternative to piezoelectric transducers in many applications.**

I. Introduction

Ultrasound is used in a wide variety of applications that can be characterized as either sensing modalities or actuating modalities. Sensing applications include medical imaging, nondestructive evaluation (NDE), ranging, and flow metering. Practical uses of ultrasound as an actuating mechanism include industrial cleaning, soldering, and therapeutic ultrasound (heating, lithotripsy, tissue ablation, etc.). Current theoretical understanding indicates, however, that many fruitful applications of ultrasound remain unrealized. Often a lack of adequate transducers precludes theoretically interesting ultrasonic systems from materializing. Thus, we find ourselves at a familiar point in the scientific process; practical applications motivate technological progress; and the technological progress, if realized, can serve to further refine theory. Specifically, air-coupled ultrasonic inspections motivate the development of air transducers [1]–[5] and the advantages of limited diffraction beams motivate the realization of 2-dimensional transducer matrices [6]–[8]. In this paper, we present micromachined ultrasonic transducers (MUTs) and report that they overcome many of the current transducer problems. MUTs are shown to work in air with the largest dynamic range reported to date, they are shown to work in water, and simulations are used to demonstrate that optimized immersion MUTs can perform comparably to piezoelectric transducers with fewer practical limitations.

In order to harness the practical potential of ultrasound, waves must be efficiently launched at, or in, the subject of interest. In all sensing applications and most actuating applications, the waves also need to be detected. Ultrasound is usually introduced into and detected from the subject via a coupling medium; it is rare for the vibrating element of the transducer to be placed in direct contact with the subject [9]. The coupling medium can be solid, such as the quartz rods used in wafer temperature measurements [10], [11]; it can be liquid, as in many NDE and medical applications, or it can be gaseous, as in air-coupled applications. Ultrasonic excitation and detection also can occur on the subject via laser light [12]–[14]. Currently, the vast majority of ultrasonic transducers are fabricated using piezoelectric crystals and composites. When performing ultrasonic investigations directly on solids, piezoelectric transducers are the best choice because the acoustic impedance of the piezoelectric ceramic is of the same order of magnitude as that of the solid. Laser based ultrasound also performs well with solids. However, when the objective is to excite and detect ultrasound in fluids (as is the case in most applications), piezoelectric transducers have drawbacks that motivate our approach to transducer design.

Piezoelectric transducers are problematic in fluid-coupled applications because of the impedance mismatch between the piezoelectric and the fluid of interest. In air, for example, the generation of ultrasound is challenging because the acoustic impedance of air (400 kg/m^2s) is many orders of magnitude smaller than the impedance of piezoelectric materials commonly used to excite ultrasonic vibrations (approximately 30×10^6 kg/m^2s). The large impedance mismatch implies that piezoelectric air transducers are inherently inefficient. In order to improve efficiency, a matching layer is usually placed in between the piezoelectric and the air [9]. The matching layer solution is problematic for three reasons. First, the impedance mismatch is so large that matching layer materials with the necessary characteristic impedance are rarely available. Second, the improved energy coupling comes at the expense of bandwidth. Third, high frequency transducers require impractically thin matching layers. Attempts to maximize the energy transfer from the piezoelectric element to the air and vice versa have achieved moderate success. However, the increased complexity of the more efficient devices reduces their reliability and increases their cost.

In the case of water-coupled ultrasound, the impedance mismatch is not as severe (approximately 30×10^6 kg/m^2s

Manuscript received May 6, 1997; accepted November 20, 1997.

I. Ladabaum, X. Jin, H. T. Soh, and B. T. Khuri-Yakub are with the E. L. Ginzton Laboratory, Stanford University, Stanford, CA 94305 (e-mail: igal@macro.stanford.edu).
A. Atalar is with Bilkent University, Ankara, Turkey.

0885–3010/98$10.00 © 1998 IEEE

for piezoceramics versus 1×10^6 kg/m^{2}s for water), but nevertheless leads to system limitations. Matching layers are still necessary, and both the ceramic and the matching layers need to be manufactured to tight mechanical tolerances. Thus, theoretically interesting designs, such as complex arrays, are limited to realizable configurations.

Piezoelectric transducers have some drawbacks in addition to the impedance mismatch problem. Because a piezoelectric's frequency range of operation is determined by its geometry, the size and frequency requirements of certain systems may not converge to a realizable configuration. Furthermore, the device's geometry defines its electrical impedance, so that sensitive receiving electronics may be forced to operate with loads that worsen their noise performance. Two-dimensional transducer matrices present particular problems because the element size required results in an electrical element impedance that does not match conventional driving and receiving electronics. Attempts to match this impedance better, such as through the use of multilayer piezoelectrics, lead to significant cross-coupling [7]. In addition, piezoelectrics are limited to strain levels of approximately 10^{-4}, which translates to a surface displacement limit of approximately 0.5 μm in the low MHz range. Such amplitudes may not be sufficient in certain gas applications. The more widely available piezoelectric ceramics depole at relatively low temperatures (approximately 80°C), which prevents them from being used in high temperature environments, while specialized ceramics that depole at higher temperatures have lower coupling constants and are very costly.

Although piezoelectric ceramics and engineering cleverness have generated a significant number of ultrasonic devices and systems, many modern applications would benefit from transducers based on a different principle of actuation and detection. Capacitive MUTs overcome many of piezoelectric transducers' drawbacks.

II. Previous Work

Analyses of capacitive acoustic transducers have existed for many decades [15], [16]. The use of capacitive transducers for airborne ultrasonics dates back to the 1950s [17], [18], and the first immersion version appeared in 1979 [19]. The use of air-coupled ultrasound in the context of NDE is also not new [1], [20], [21]. Recently, a report has been published describing air-coupled longitudinal wave excitation in metals at frequencies below 1 MHz [22].

The application of micromachining techniques to fabricate acoustic transducers consisting of suspended membranes over a backplate was reported within the last decade [23]. Recently, papers have been published describing various designs and models of capacitive ultrasonic air transducers [24]–[27]. However, the papers generally omit models that are adequate for the design of optimized transducers, and a robust explanation of the operation of the devices is usually lacking. More rigorous modeling of grooved backplate electrostatic transducers has been published [28], but the transducers it describes are limited to 500 KHz operation. A capacitive ultrasonic transducer made with more advanced fabrication technology was invented in 1993 [29]–[31]. The capabilities, fabrication procedures, and modeling of the device have been improved [32]–[36] and have spurred concurrent development efforts [37]. The present state of such transducer development, including a more thorough theoretical treatment than in previous publications, is the subject of this paper.

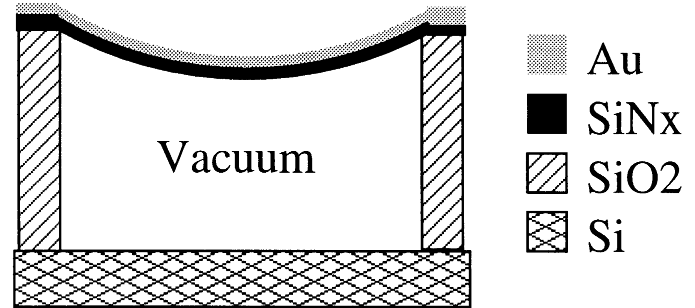

Fig. 1. Schematic of one element of a MUT.

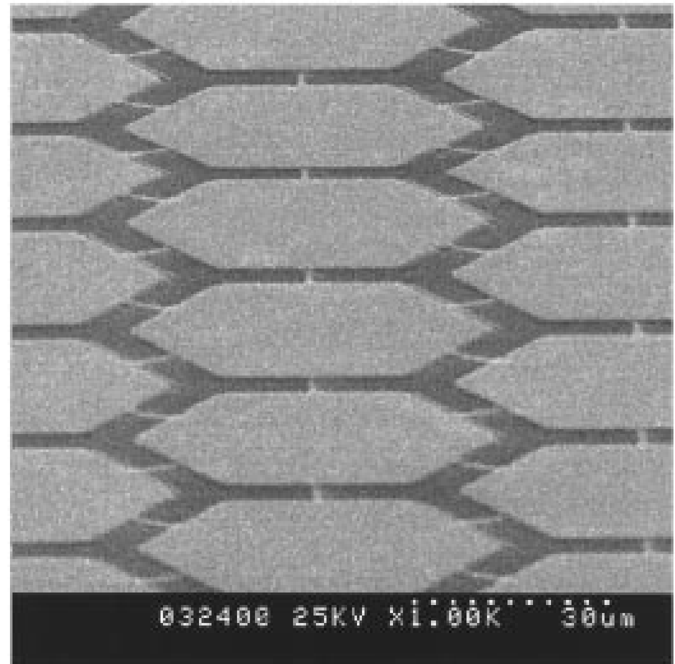

Fig. 2. SEM of a portion of a MUT.

III. Device Description

A MUT consists of metalized silicon nitride membranes suspended above heavily doped silicon bulk. A schematic of one element of the device is shown in Fig. 1. A transducer consists of many such elements, as shown in the scanning electron microscope (SEM) image of Fig. 2. When a voltage is placed between the metalized membrane and the bulk, coulomb forces attract the membrane toward the bulk and stress within the membrane resists the attraction.

If the membrane is driven by an alternating voltage, significant ultrasound generation results. Conversely, if the membrane is biased appropriately and subjected to ultrasonic waves, significant detection currents are generated. Micromachining is the chosen vehicle for device fabrication because the membrane's dimensions (microns) and residual stress (hundreds of MPas) can be precisely controlled. Silicon and silicon nitride have excellent mechanical properties, and can be readily patterned using the wide repertoire of procedures invented by the semiconductor industry.

Certain qualitative observations about MUT design are worth noting. If the energy associated with a transducer's surface motion when unloaded is low compared to the energy associated with the surface motion when loaded by the medium of interest (e.g., air, water), the transducer then will have a broad bandwidth. Thus, when operation is intended in lower density media, the surface of motion should be associated with a light structure. The structure can be made resonant to further enhance energy transfer at the expense of some bandwidth. Our thin resonant membrane fits these criteria. Also important to the electromechanical coupling of a transducer is the fact that large coulombic forces are realized when an electrical potential is applied across a small gap. Thus, a thin metalized membrane separated from a conducting backplate by a small gap is a critical feature of our design. Because detection entails measuring the fractional change of the MUT capacitance when ultrasonic waves impinge on it, a small gap is also desirable in order to maximize detection sensitivity. Furthermore, to avoid both electrical breakdown and the mechanical effects of backside air loading, the transducer cavity can be evacuated. It is important to realize that optimization of transducer design need not be limited to a single solution; a transducer can be optimized for emission, and a different transducer can be optimized for reception. For example, a sensitive receiver would be made with a thin gap, which would limit its power output as an emitter. Thus a thin gap receiver and a thicker gap emitter could each be optimized in a final system.

IV. MUT Fabrication

MUTs are fabricated by using techniques pioneered by the integrated circuits industry. A fabrication scheme of the MUTs used to generate some of the results reported herein[1] is found in Fig. 3.

A p-type (100) 4 in. silicon wafer is cleaned, and a 1 μm oxide layer is grown with a wet oxidation process. A 3500 Å layer of LPCVD nitride is then deposited. The residual stress of the nitride can be varied by changing the proportion of silane to ammonia during the deposition process. The residual stress used is approximately 80 MPa. A pattern of etchant holes is then transferred to the wafer with an electron beam lithography process. The nitride is plasma etched, and the sacrificial oxide is removed with HF. Note that the etchant holes define the elements' geometry,[2] as is shown in Fig. 4. A second 2500 Å layer of LPCVD nitride is then deposited on the released membranes, vacuum sealing the etchant holes. The holes are patterned with an electron beam so that their small size allows for adequate sealing of the cavity. A chrome adhesion layer and a 500 Å film of gold are evaporated onto the wafer.

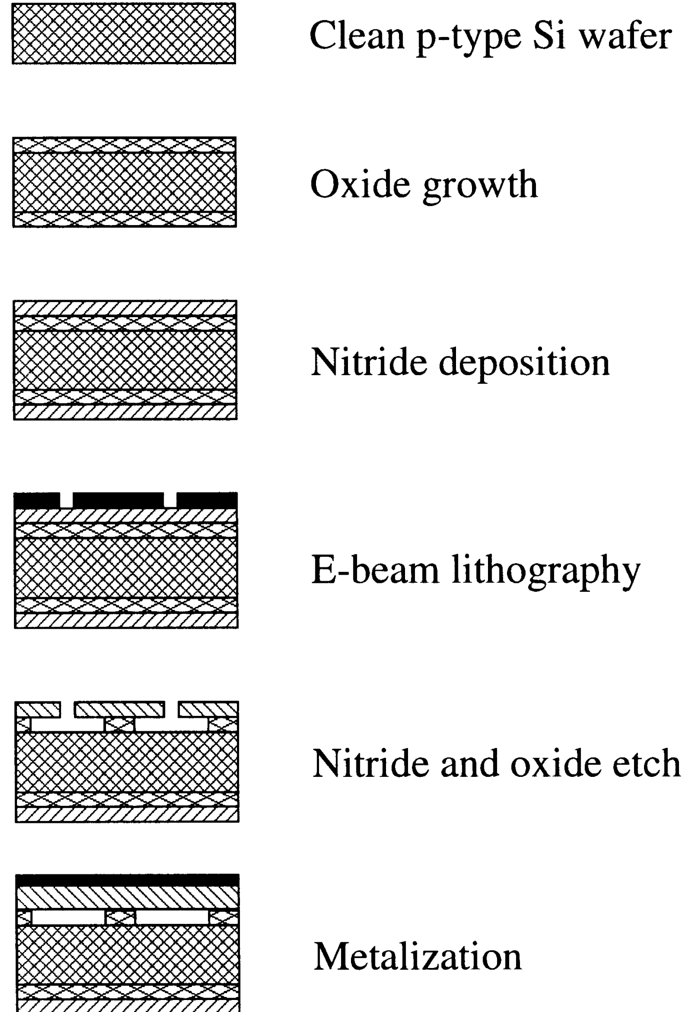

Fig. 3. Major steps of MUT fabrication.

The wafer is then diced, and the MUTs are mounted on a circuit board with epoxy. A gold wire bond connects the top electrode to the circuit board. In an older process, conductive epoxy was used to make contact to the bulk of the silicon (the lower electrode). Currently, a wire bond also connects the lower electrode to the circuit board.

V. Theory

In both the analysis and design of MUTs, it is important to differentiate between a MUT as a receiver and a

[1] Other fabrication schemes are currently being reduced to practice and are the subject of upcoming conference proceedings [36].

[2] Some devices were fabricated with hexagonally close packed membranes, whereas some results were obtained with circular membranes.

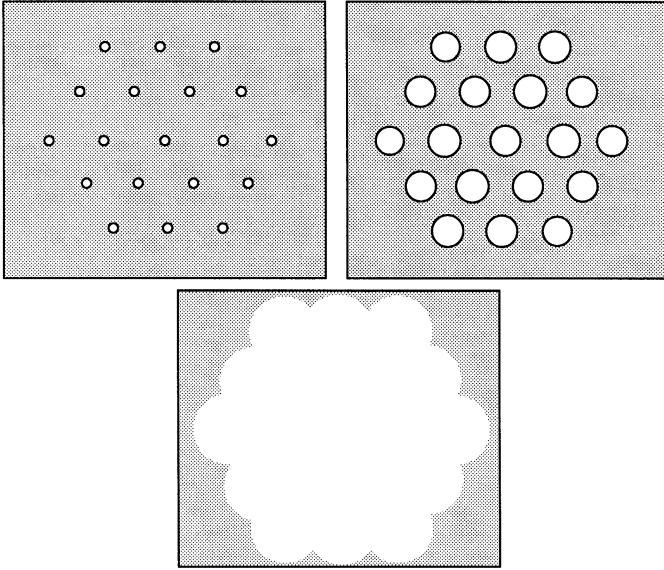

Fig. 4. Time lapse of sacrificial etch.

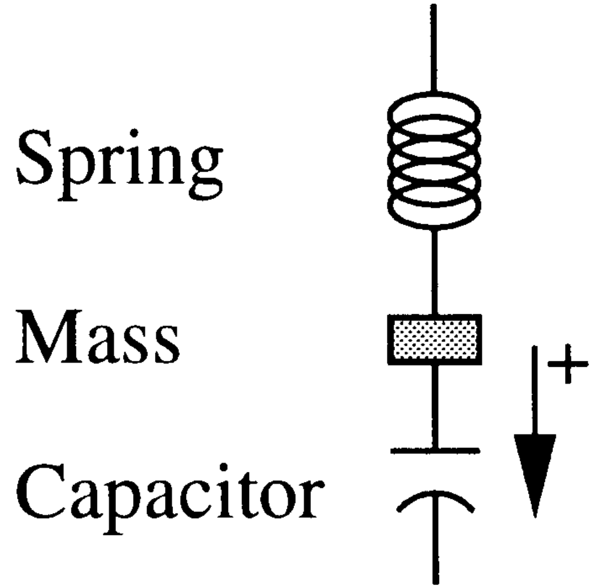

Fig. 5. First order lumped electro-mechanical model of a MUT element.

MUT as an emitter. The purpose of a receiving MUT is to detect the small ultrasonic signals that result after insonification of a sample. Thus, a linearized small signal analysis is appropriate. In contrast, the aim of an emitting MUT is to launch ultrasonic waves of sufficient magnitude to enable applications of interest. Hence, the displacement of the emitting MUT's membrane can be large, and a more involved nonlinear analysis is necessary to quantitatively predict a collapse voltage and an electromechanical coupling factor. In this section, we present a first order analysis of an emitting MUT. We then present a small signal model that yields a quantitative description of a receiving MUT.

A. First-order Analysis

Several approximations simplify the analysis and serve to highlight the most significant aspects of MUT behavior. We assume that the membrane's restoring force is a linear function of its displacement. We neglect all electrical fringing fields and membrane curvature when considering the electrical forces on the membrane. Furthermore, we take all conductors and contacts to be perfect. We then assume that the MUT operates in a vacuum, which is equivalent to neglecting any loading of the membrane[3]. Thus, we obtain a lumped electro-mechanical model consisting of a linear spring, a mass, and a parallel plate capacitor, as shown in Fig. 5.

The mass is actuated by the resultant of the capacitor and spring forces.

$$F_{\text{capacitor}} + F_{\text{spring}} = F_{\text{mass}}$$

[3]The lack of dissipative elements implies that a resonant condition would result in infinite displacement; nonetheless, dissipative loads are neglected for clarity.

The force exerted by the capacitor is found by differentiating the potential energy of the capacitor with respect to the position of the mass (principle of virtual work):

$$F_{\text{capacitor}} = -\frac{d}{dx}\left(\frac{1}{2}CV^2\right) = -\frac{1}{2}V^2\left[\frac{d}{dx}\left(\frac{\epsilon S}{d_0 - x}\right)\right] = \frac{\epsilon S V^2}{2(d_0 - x)^2} \quad (1)$$

where V is the voltage across the capacitor, C is capacitance, ϵ is the electric permittivity, S is the area of the capacitor plates, x is displacement in the direction shown in Fig. 5 and d_0 is the separation of the capacitor plates at rest. The spring exerts a force that is linearly proportional to displacement

$$F_{\text{spring}} = -kx$$

where k is the spring constant. Substituting for the force terms and noting all time dependence explicitly gives:

$$m\frac{d^2x(t)}{dt^2} - \frac{\epsilon S[V(t)]^2}{2[d_0 - x(t)]^2} + kx(t) = 0. \quad (2)$$

Equation (2) is a nonlinear differential equation of second order, and its solution is not trivial. In order to extract the significant qualitative behavior of the system, we consider the case where $V(t) = V_{DC}$, which implies no time dependence and leads to:

$$\frac{\epsilon S V_{DC}^2}{2(d_0 - x)^2} = kx. \quad (3)$$

Equation (3) can be rearranged into a third degree polynomial in x whose solution has two regions of interest. For small V_{DC}, the solution consists of three real roots, of which only one is a physical solution (the other roots correspond to an unphysical $x > d_0$ and to an unstable

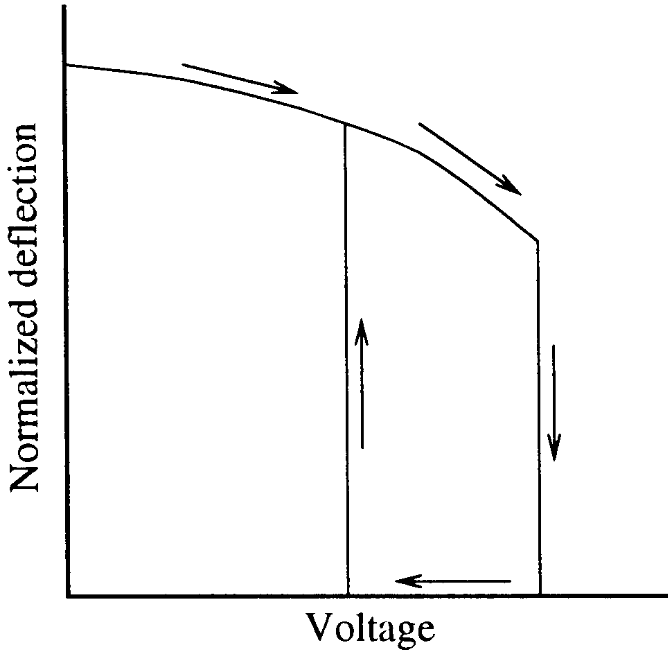

Fig. 6. Sketch of MUT hysteresis.

point). As V_{DC} is increased, there is a point at which the electrostatic force overwhelms the spring's restoring force, and the membrane collapses. This inflection point is found when there is a double real root such that $x > d_0$. The collapse point occurs when:

$$V_{\text{collapse}} = \sqrt{\frac{8kd_0^3}{27\epsilon S}}$$
$$x_{\text{collapse}} = \frac{d_0}{3}.$$

In order to prevent the capacitor from shorting after collapse, we imagine a thin insulating layer of thickness $d_{\text{insulator}}$ on one of the electrodes (the metalized membrane's nitride, in a real MUT). Note that we have neglected the effect of such an insulating layer until this point. It is possible to account for the insulator in (2) and (3), but it is conceptually more clear to assume that $d_{\text{insulator}}$ and $\epsilon_{\text{insulator}}$ can be neglected until collapse. After the membrane has collapsed, it will not snap back until the voltage is reduced below V_{collapse} to

$$V_{\text{snap-back}} = \sqrt{\frac{2kd_{\text{insulator}}^2(d_0 - d_{\text{insulator}})}{\epsilon_{\text{insulator}} S}}.$$

A sketch of such hysteretic behavior is found in Fig. 6. We conclude from such analysis that membrane collapse is a possibility, and we report in the results section that such collapse is observed.

In addition to membrane collapse, electrostatic spring softening also is observed experimentally. Such softening arises from the fact that, as the capacitor plate displaces in the $+x$ direction, a spring force is generated in the $-x$ direction. However, displacement in the $+x$ direction under constant V_{DC} also causes an increase in the electrostatic force in the $+x$ direction. This increase in electrostatic force can be interpreted as a spring softening. A more mathematical explanation begins by linearizing (2) with a Taylor expansion about the point $x(t) = 0$:

$$m\frac{d^2x(t)}{dt^2} - \left[\frac{\epsilon SV_{DC}^2}{2d_0^2} + \frac{\epsilon SV_{DC}^2}{d_0^3}x(t)\right] + kx(t) = 0. \tag{4}$$

Collecting terms yields an equation in a familiar form

$$m\frac{d^2x(t)}{dt^2} + \left(k - \frac{\epsilon SV_{DC}^2}{d_0^3}\right)x(t) = \frac{\epsilon SV_{DC}^2}{2d_0^2} \tag{5}$$

which we rewrite as

$$m\frac{d^2x(t)}{dt^2} + k_{\text{soft}}x(t) = \frac{\epsilon SV_{DC}^2}{2d_0^2} \tag{6}$$

where

$$k_{\text{soft}} = k - \frac{\epsilon SV_{DC}^2}{d_0^3}.$$

Thus, we expect to see a drop in the resonance frequency of the system as V_{DC} is increased. Such a frequency shift is observed, and reported in the results section.

Even though much is left to decipher about the complex nonlinear behavior of a MUT under large displacement conditions, small signal operation about a bias point yields fruitful practical and theoretical results. If in (1) we assume that the membrane displacement x is small compared to the gap spacing d_0, then:

$$F_{\text{capacitor}} \approx \frac{\epsilon SV^2}{2d_0^2} \propto V^2.$$

If we let $V = V_{DC} + V_{ac}$ then

$$F_{\text{capacitor}} \propto V_{DC}^2 + 2V_{DC}V_{ac} + V_{ac}^2.$$

If we choose $V_{DC} \gg V_{ac}$ then the time varying forcing function

$$F_{ac} \propto 2V_{DC}V_{ac}.$$

Thus, reasonable experiments can be performed and interpreted even though a full understanding of an emitting MUT's behavior requires further analysis.

B. Small Signal Model

In order to facilitate the design of systems enabled by MUTs, the goal of the theory is to arrive at an equivalent circuit model of the transducer. The equivalent circuit should be a two port network, where the electrical domain (voltage and current) is represented at one port, and the mechanical domain (force and velocity) is represented at the other port. The equivalent circuit is valid under small signal conditions for a receiving MUT, and even for an emitting MUT, as long as the membrane displacement is not near the collapse point and the bias voltage does not cause significant spring softening. The approach,

as first suggested by Mason [15], is to find the mechanical impedance of the membrane in vacuum and then to insert it in a transformer equivalent circuit. Because the first membranes we fabricated were circular, and also to facilitate analytical treatment, we consider the circular membrane solution. We hypothesize that hexagonal membrane behavior is approximated well by circular membrane behavior. We use Mason's derivation with some corrections, and preserve his notation as much as possible.

C. Mechanical Impedance of a Membrane in Vacuum

We consider a circular membrane of radius a operating in vacuum. The membrane has a Young's modulus of Y_0 and a Poisson's ratio of σ. In addition, the membrane is in tension T in units of N/m^2. The differential equation governing the normal displacement $x(r)$ of the membrane can be written as [15], [38]:

$$\frac{(Y_0+T)l_t^3}{12(1-\sigma^2)}\nabla^4 x(r) - l_t T\nabla^2 x(r) - P - l_t\rho\frac{d^2x(r)}{dt^2} = 0 \quad (7)$$

where l_t is the membrane thickness, and P is the external uniform pressure applied to the membrane. The equation is derived from an energy formulation, and the critical assumption is that the tension generated by a displacement x is small compared to the tension T. Assuming a harmonic excitation at an angular frequency ω, (7) is known to have a solution of the form:

$$x(r) = AJ_0(k_1 r) + BJ_0(k_2 r) + CK_0(k_1 r) + DK_0(k_2 r) - P/(\omega^2\rho l_t) \quad (8)$$

where A, B, C, and D are arbitrary constants, $J_0()$ is the zeroth order Bessel function of the first kind, and $K_0()$ is the zeroth order Bessel function of the second kind. We immediately deduce that $C = 0$ and $D = 0$ because the Bessel function of the second kind is infinite at $r = 0$, which is not physical. If we use (8) to substitute for $x(r)$ in (7), we find that k_1 and k_2 must satisfy the characteristic equations:

$$\frac{(Y_0+T)l_t^2}{12(1-\sigma^2)}k_1^4 + \frac{T}{\sigma}k_1^2 - \omega^2 = 0 \quad (9)$$

$$\frac{(Y_0+T)l_t^2}{12(1-\sigma^2)}k_2^4 + \frac{T}{\sigma}k_2^2 - \omega^2 = 0. \quad (10)$$

Following Mason's notation, we define

$$c = \frac{(Y_0+T)l_t^2}{12(1-\sigma^2)} \quad \text{and} \quad d = \frac{T}{\rho}. \quad (11)$$

The quadratic formula then gives the solutions:

$$k_1 = \sqrt{\frac{\sqrt{d^2+4c\omega^2}-d}{2c}} \quad \text{and} \quad k_2 = j\sqrt{\frac{\sqrt{d^2+4c\omega^2}+d}{2c}}. \quad (12)$$

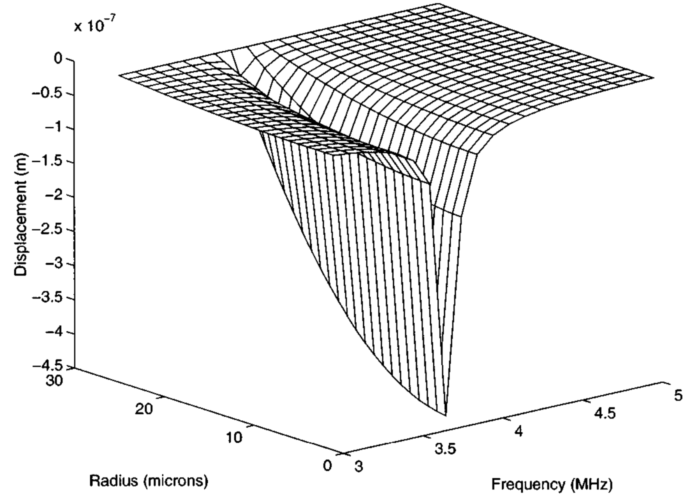

Fig. 7. Calculated displacement as a function of frequency for a 25 μ membrane excited by uniform pressure.

In order to determine the constants A and B, two boundary conditions are necessary. Physically reasonable boundary conditions at $r = a$ are that $x = 0$, which implies that the membrane undergoes no displacement at its periphery, and $(d/dr)x = 0$, which implies that the membrane is perfectly flat (i.e., does not bend) at it's periphery. Both conditions amount to stating that the membrane is perfectly bonded to an infinitely rigid substrate. Using these conditions, we determine the constants A and B and find the displacement of the membrane as:

$$x(r) = \frac{P}{\omega^2\rho l_t} \times \left[\frac{k_2 J_0(k_1 r)J_1(k_2 a) + k_1 J_0(k_2 r)J_1(k_1 a)}{k_2 J_0(k_1 a)J_1(k_2 a) + k_1 J_1(k_1 a)J_0(k_2 a)} - 1\right]. \quad (13)$$

Fig. 7 is a calculated plot of the displacement of a typical membrane as a function of frequency under a uniform pressure excitation[4]. For the simulation, values used were $a = 25\times10^{-6}$, $l_t = 0.6\times10^{-6}$, $P = 1$, $Y_0 = 3.2\times10^{11}$, $\sigma = 0.263$, $T = 280\times10^6$, and $\rho = 3270$ (all in MKS units).

Because we have assumed uniform pressure P, the force on the membrane is simply PS, where S is the area of the membrane. The velocity of the membrane is $v(r) = j\omega x(r)$, and we take $\overline{v}$ as the lumped velocity parameter where:

$$\begin{aligned}\overline{v} &= (1/\pi a^2)\int_0^a\int_0^{2\pi} v(r)r\,d\theta\,dr \\ &= \frac{jP}{\omega\rho l_t} \times \left[\frac{2(k_1^2+k_2^2)J_1(k_1 a)J_1(k_2 a)}{ak_1k_2(k_2J_0(k_1a)J_1(k_2a)+k_1J_1(k_1a)J_0(k_2a))} - 1\right].\end{aligned} \quad (14)$$

Mechanical impedance is defined as the ratio of pressure to velocity. Hence, the mechanical impedance of the mem-

[4]Fig. 7 illustrates the mechanical resonance of the membrane. The displacement in this particular example is too large to be valid for the small signal equivalent circuit derived in the next section.

$$Z_m = \frac{P}{\overline{v}} = j\omega\rho l_t \left[\frac{l_t a k_1 k_2 (k_2 J_0(k_1 a) J_1(k_2 a) + l_t k_1 J_1(k_1 a) J_0(k_2 a))}{a k_1 k_2 (k_2 J_0(k_1 a) J_1(k_2 a) + k_1 J_1(k_1 a) J_0(k_2 a)) - 2(k_1^2 + k_2^2) J_1(k_1 a) J_1(k_2 a)} \right]. \tag{15}$$

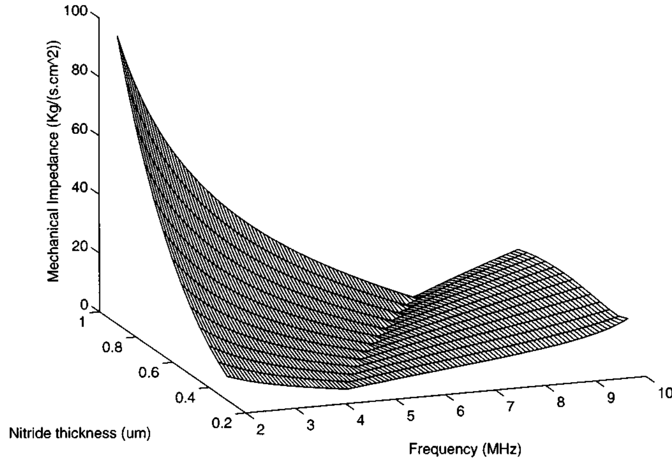

Fig. 8. Calculated absolute value of mechanical impedance for a silicon nitride membrane as a function of frequency and thickness.

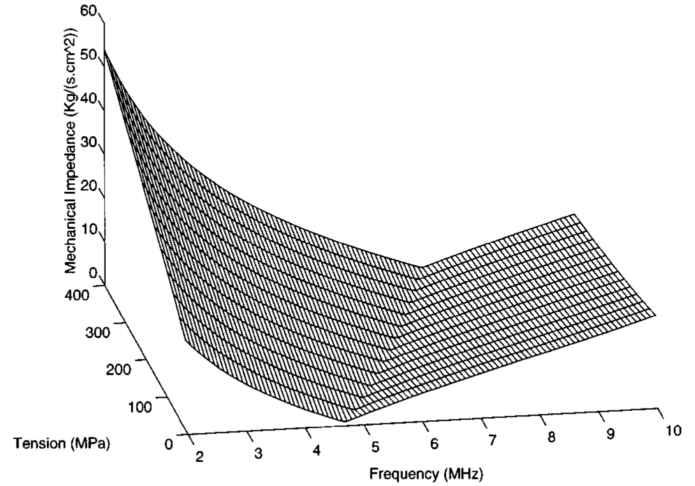

Fig. 9. Calculated absolute value of mechanical impedance as a function of frequency and membrane tension.

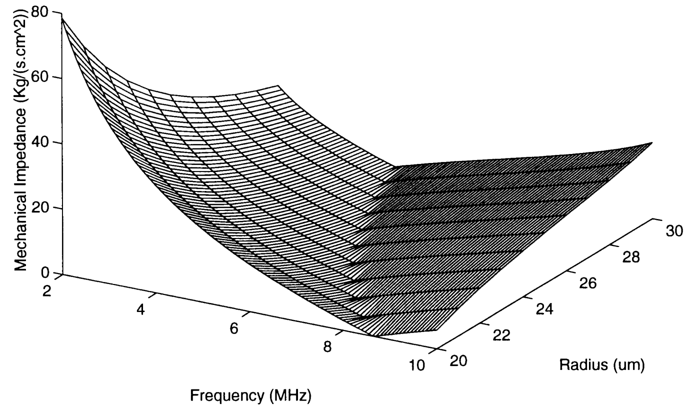

Fig. 10. Calculated absolute value of mechanical impedance for a silicon nitride membrane as a function of frequency and radius.

brane, Z_m, can be written as: (see equation 15).[5] Figs. 8, 9, and 10 show calculated values of this impedance as a function of each critical parameter. In each figure, all parameters except the one of interest are held constant. The significance of Figs. 8, 9, and 10 is that they demonstrate how a MUT membrane's impedance can be tailored to be insignificant compared to the medium's acoustic impedance, which is the necessary condition for efficient power transfer.

D. Electrostatically Excited Membrane and Its Equivalent Circuit

The membrane of thickness l_t is coated with a thin layer of conducting material on the top side, and the bottom electrode is separated from the membrane by a distance l_a. The electrical capacitance can be written as:

$$C(t) = \frac{\epsilon_0 \epsilon S}{\epsilon_0 l_t + \epsilon l_a(t)} \tag{16}$$

where ϵ is the dielectric constant of the membrane material, and S is the area of the membrane. If a DC voltage V_{DC} is applied between the top electrode and the bottom, the electrostatic attraction force on the membrane is given by:

$$F_E = -\frac{d}{dx}\left(\frac{1}{2} C V_{DC}^2\right) = \frac{\epsilon_0 \epsilon^2 S V_{DC}^2}{2(\epsilon_0 l_t + \epsilon l_a)^2}. \tag{17}$$

[5]The choice of lumped parameters for distributed systems can be subtle. A lumped mechanical impedance in series with a lumped radiation impedance must adequately describe the power delivered to the medium. Because our analysis is predicated on a small signal approximation, we do not introduce a rigorous solution here, but it should nonetheless be pointed out that rigorous lumped parameters for apodized transducers can be obtained.

Let the total voltage across the capacitor be $V = V_{DC} + V_{ac}\sin(\omega t)$, where V_{DC} is the bias voltage and $V_{ac} \ll V_{DC}$ is the small signal AC voltage. Then, the current flowing through the device is:

$$I = \frac{d}{dt} Q = \frac{d}{dt}\left(C(t) V(t)\right) = C(t)\frac{d}{dt} V(t) + V(t)\frac{d}{dt} C(t). \tag{18}$$

Because this is a small signal analysis, we also can assume that the capacitor can be described by $C(t) = C_0 + C_{ac}\sin(\omega t + \phi)$ where $C_{ac} \ll C_0$. We can then rewrite (18) as:

$$I = C_0 \frac{d}{dt} V_{ac}(t) + V_{DC}\frac{d}{dt} C_{ac}(t). \tag{19}$$

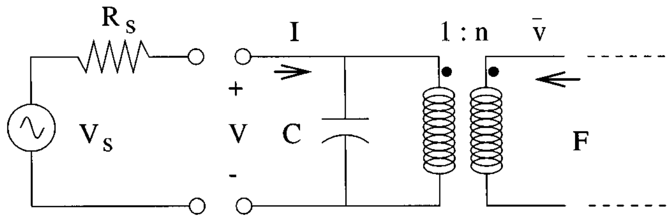

Fig. 11. Partial electrical equivalent circuit of MUT.

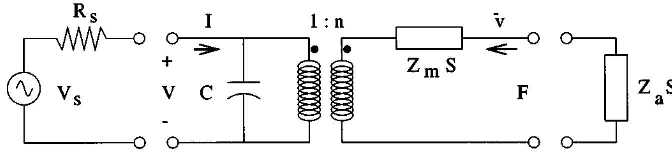

Fig. 12. Electrical equivalent circuit of MUT.

If we differentiate (16) we obtain:

$$\frac{d}{dt}C_{ac}(t) = -\frac{\epsilon_0\epsilon^2 S}{(\epsilon_0 l_t + \epsilon l_{a_0})^2}\frac{d}{dt}l_a(t) \tag{20}$$

where l_{a_0} is the DC value of the gap spacing. The derivative of the air gap thickness is equal to membrane velocity $(d/dt)l_a = \overline{v}$, which leads to:

$$I = C_0\frac{d}{dt}V_{ac}(t) - \frac{V_{DC}\epsilon_0\epsilon^2 S}{(\epsilon_0 l_t + \epsilon l_{a_0})^2}\overline{v}. \tag{21}$$

Equation (21) is significant because it transforms velocity, a mechanical quantity, into electrical current. Thus, we can define a transformer ratio:

$$n = \frac{V_{DC}\epsilon_0\epsilon^2 S}{(\epsilon_0 l_t + \epsilon l_{a_0})^2} \tag{22}$$

and write the current as sum of electrical and mechanical components

$$I = C\frac{d}{dt}V_{ac}(t) - n\overline{v}. \tag{23}$$

It is important to note that n can be controlled by varying the applied bias voltage or by changing the membrane and air gap thickness. Using (23) we can draw the partial small signal equivalent circuit shown in Fig. 11.

In order to complete the equivalent circuit, a relationship between force and velocity at the mechanical port is necessary. By definition, an equivalent load impedance constitutes such a relationship. By inspection, and using the mechanical impedance of (15), the equivalent circuit of Fig. 12 is obtained. The impedance elements are placed in series in order to maintain consistency with definitions. For example, the load impedance of vacuum is zero, so it must be placed in series with the membrane impedance because a parallel combination would imply a total load of zero.

When loaded by air, the bandwidth of the transducer is dominated by the mechanical impedance of the membrane. As shown in the results section, the typical 3 dB bandwidth of an air-loaded transducer is 5% of the center frequency. The bandwidth can be further increased at the cost of efficiency.

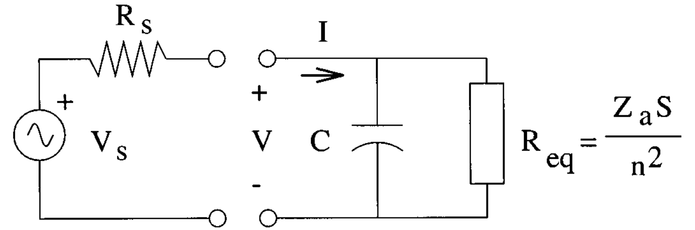

Fig. 13. Electrical equivalent circuit of MUT when $Z_m \ll Z_a$.

In contrast to an air-loaded transducer, an immersion MUT has its bandwidth determined by the transformer ratio. In most configurations of a MUT element, the mechanical impedance of the immersion medium, Z_a, is much greater than the membrane impedance, Z_m. In this case the equivalent circuit of the MUT simplifies to that shown in Fig. 13, where the equivalent resistance is given by:

$$R_{eq} = Z_a S/n^2 = Z_a\frac{(\epsilon_0 l_t + \epsilon l_a)^4}{V_{DC}^2\epsilon_0^2\epsilon^4 S}. \tag{24}$$

The Q factor of the MUT is thus given by:

$$Q = \omega R_{eq} C = \frac{\omega Z_a(\epsilon_0 l_t + \epsilon l_a)^3}{V_{DC}^2\epsilon_0\epsilon^3} \text{ for } Z_m \ll Z_a. \tag{25}$$

It is clear that, for wide band operation, l_t and l_a should be chosen as small as possible, and the DC bias voltage V_{DC} should be kept as high as possible. The bias voltage, however, is limited by the collapse voltage (discussed in the first order analysis). Thus, there exists a lower bound on the quality factor. The determination of this lower bound entails more involved nonlinear analysis, and it is the subject of current research. Nonetheless, a conservative assumption is that a configuration with parameters $l_t = 0.3\ \mu$m, $l_a = 0.2\ \mu$m, and $V_{DC} = 80$ V does not collapse. Such a configuration has a Q, according to (25), of 23.

The electrical equivalent circuit allows analysis and optimization of the MUT structure. Furthermore, circuits can be designed to tune a particular transducer. As is shown in the results section, the model agrees well with experimental observations. Nevertheless, the model does not take into account several factors. There is no term to represent the mechanical impedance of the cavity behind the membrane, nor of the supporting structure, which can present significant real and imaginary loads. Also absent are terms for the parasitic electrical elements present in any real device. The careful derivation of such terms, as well as the investigation of the nonlinear nature of the device when operated at large displacements, are topics of current research.

VI. Results

The present results, which include air-coupled through-transmission of aluminum, constitute a significant improvement over previously reported results [32]–[35]. The transmission results herein presented are generated with a simple experimental setup. A function generator and voltage source excite the emitter, and a custom transconductance amplifier with approximately 40 dB of gain detects the signal at the receiver. When appropriate, a series inductor is used to tune the transducer to match the electronics' impedance. The signal is digitized by an 8 bit digitizing oscilloscope, and it is transferred to a computer for display. The impedance curves herein reported are taken with an HP 8752A network analyzer connected to the biased transducer with a bias-T. The theoretical curves are generated by a computer program that incorporates the theory developed in this paper.

In preliminary transmission experiments with no aluminum slab present, transducer membranes were observed to transmit at a low frequency of 1.8 MHz (100 micron membrane) to a high frequency of 12 MHz (12 micron membrane). Fig. 14 shows the ultrasound detected after passing through air, then into a 1.9 mm slab of aluminum (longitudinal mode), then air. The excitation was at the 2.3 MHz resonance frequency of the transducer, and consisted of a 20 cycle tone burst of 16 V riding on a bias of 30 V. The received signal was averaged 16 times, and presents a 30 dB signal-to-noise ratio. The emitter had dimensions of 1 cm^2, the receiver was 0.25 cm^2, and the transducers were placed 1 cm apart. Because the aluminum slab causes 70 dB of signal loss, 0.8 cm of air cause 5 dB of loss, and electrical impedance mismatch between the transducer and the receiving electronics cause an additional 5 dB of loss, the transducer dynamic range is approximately 110 dB[6]. The dynamic range of 110 dB was further verified by removing the aluminum and reducing the excitation voltage of the emitter until it was barely detectable at the receiver, which occurred at 0.2 mV. Thus, assuming a linear variation of power with excitation voltage, the range from 0.2 mV to 16 V represents 98 dB of dynamic range. The 5 dB electrical impedance mismatch and a loss of 6 dB from 1 cm of air contribute to a total dynamic range of 109 dB; 16 V is taken as the upper limit of excitation power because it was the highest voltage used in the experiments and it is the approximate limit of a linearized analysis. It is possible that the transducers' dynamic range actually exceeds 110 dB.

The transducers used for the aluminum experiment were unsealed. However, a vacuum sealed pair of transducers is able to operate in both water and air. Water transmission is shown in Fig. 15 for transducers placed 0.5 cm apart. When the noise floor of the receiver was measured, it was found to be 60 dB below the peak received signal (the receiving MUT's capacitance was tuned out with a series inductor). Interesting features of Fig. 15 are the acoustic echoes, which indicate that the receiver's acoustic impedance is not perfectly matched to water. Such a mismatch implies a loss in efficiency, and it is due to unoptimized electrical tuning and physical construction. A MUT is comprised of thousands of active elements joined by supporting structure. The inactive supporting structure is responsible for reduced efficiency, so its surface area should be minimized in future designs. When the devices are operated untuned, they exhibit a fractional bandwidth in excess of 100%. The same pair of transducers was used to observe transmission from 1 to 20 MHz, but the signal was almost at the noise level at the high frequencies. The design of the devices used for water transmission was not

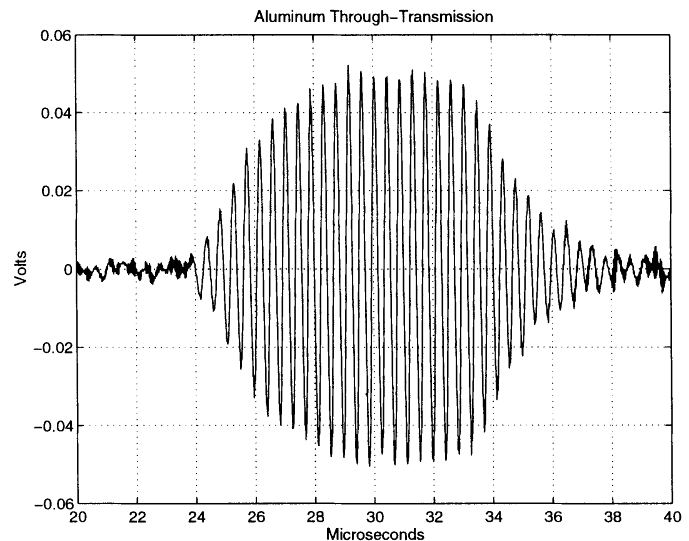

Fig. 14. Air coupled aluminum through-transmission at 2.3 MHz.

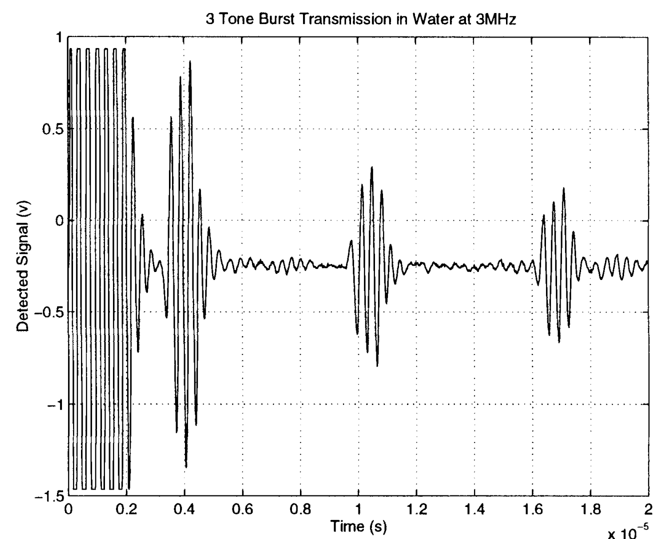

Fig. 15. Water transmission at 3 MHz.

[6]The acoustic properties of aluminum are taken from [9] and are used in the well-known formula for the power transmission coefficient (see for example [39]) to predict the 70 dB of mismatch loss. It should be noted that a 1.9 mm slab of aluminum is far from its thickness mode resonance, thus giving a large loss factor. Experiments performed since the original submission of the manuscript with 1.6 mm of steel also verify 110 dB of dynamic range. Details of steel results will be presented in future publications.

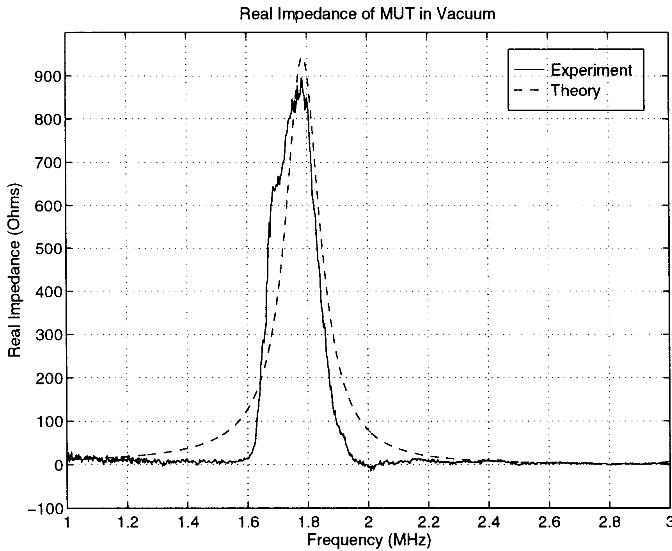

Fig. 16. Real part of impedance under vacuum: experiment and theory.

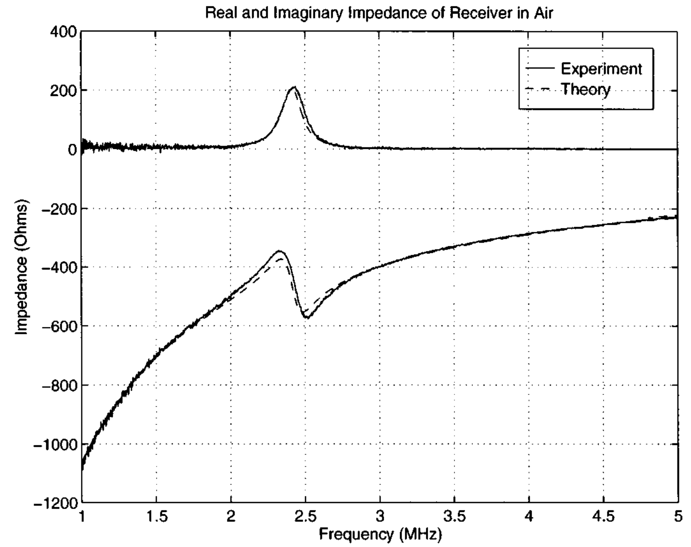

Fig. 17. Impedance in air: experiment and theory.

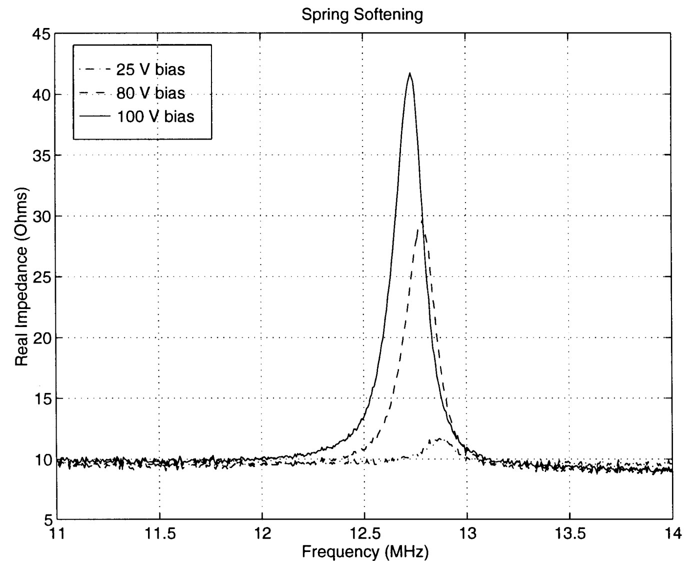

Fig. 18. Evidence of spring softening: change in resonant frequency with bias voltage.

optimized. It is anticipated that future generations of devices, based on the analysis herein reported, will approach the dynamic range of piezoelectric devices [34].

The transmission experiments show that practical applications of MUTs are feasible. In fact, the aluminum results show that air-coupled ultrasound is likely to play an increasingly important role in nondestructive testing. The water transmission results show that the significant advantages of microfabrication (on chip electronics, cost, repeatability) may soon find their way into the ultrasonic transducer industry.

The more significant result from an academic point of view, however, is that the theoretical model of the device agrees well with experimental observation. Fig. 16 shows good agreement between the measured and simulated values of the real electrical impedance of the receiving transducer used in the aluminum experiment. The small discrepancy can be attributed to the approximations in the model, the most significant of which is that the hexagonal membranes can be treated as circular membranes. The parameters used in the program agree with the expected parameters of the fabrication process ($l_t = 0.6$ μm, $l_a = 0.75$ μm, $T = 170$ MPa, $a = 48$ μm). In order to fit the theory to the experiment, a load of 3000 Ohms was placed on the acoustic port of the circuit model. This load represents all acoustic losses in vacuum. When this loss load is also used in an air impedance experiment, excellent agreement exists with theory[7] (see Fig. 17).

Confirmation of behavior predicted by the first order analysis was also obtained. Fig. 18 shows a decrease in resonant frequency with increasing voltage. This change in frequency is due to an effective softening of the spring, as has been explained.

Figs. 19 and 20 demonstrate the hysteretic collapse behavior predicted in Fig. 6. As the bias voltage is increased, the baseline of the imaginary impedance shifts, implying the reduction of gap spacing. When the voltage is increased beyond 40 V, the characteristic signature of resonance disappears, and no further change is observed. The membrane does not snap back until the voltage is reduced well below the collapse voltage[8].

Because our theoretical understanding is verified by experiment, we are basing future transducer designs on the theory herein reported. It is a critical feature of MUTs that their geometric characteristics (gap thickness, membrane thickness and radius) can control their electrical impedance. Thus, transducers can be made to match the most sensitive electronics available at a center frequency of

[7] A change in the tension parameter was made to reflect the increased stiffness of an air-backed membrane versus a vacuum backed membrane.

[8] The membrane used to generate Fig. 19 is thicker than the one that generated Fig. 17, which explains the difference of resonance frequencies.

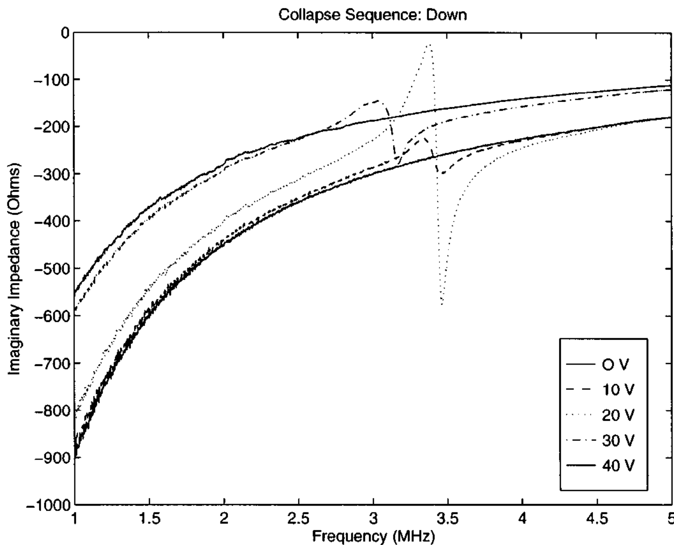

Fig. 19. Evidence of membrane collapse: imaginary impedance as a function of bias voltage.

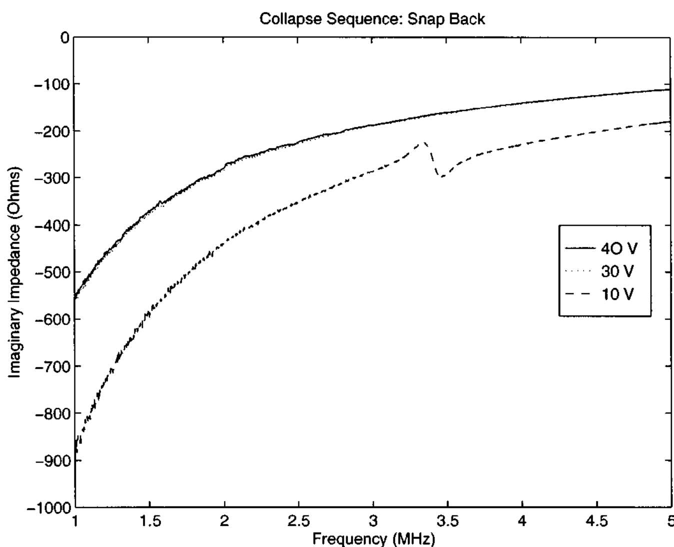

Fig. 20. Evidence of hysteresis: imaginary impedance as a function of bias voltage.

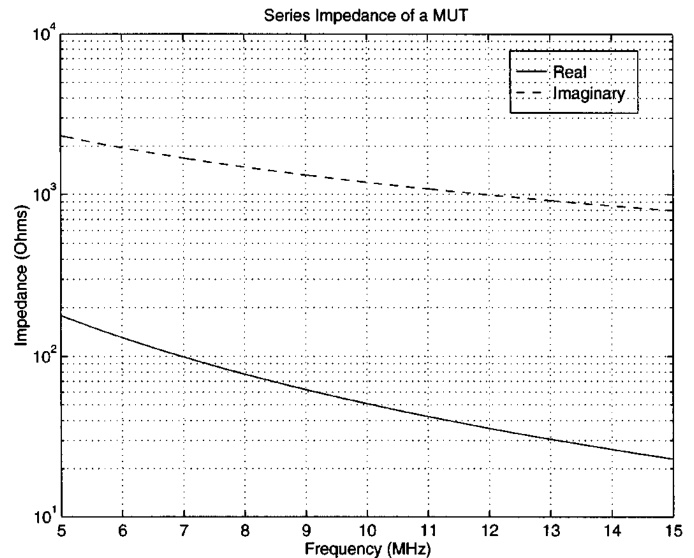

Fig. 21. Simulation of a 50 Ω immersion device (a = 10 μm, l_a = 0.2 μm, l_t = 0.3 μm, V_{DC} = 80 V).

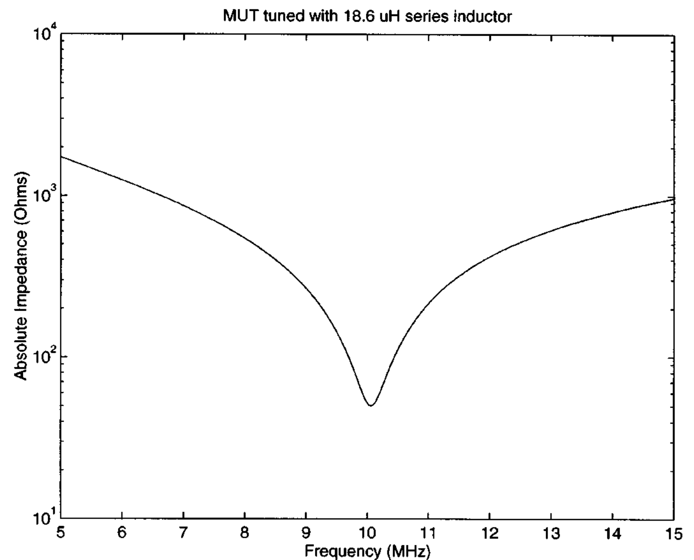

Fig. 22. Tuned immersion device (a = 10 μm, l_a = 0.2 μm, l_t = 0.3 μm,V_{DC} = 80 V, L = 19 μH).

interest. Currently, we plan to fabricate transducers with a 50 Ω real impedance, which would allow them to be used with readily available electronic components. The simulated impedance of a proposed design is found in Fig. 21.

As has been explained, the bandwidth of the device is greatest when the bias voltage is as large as possible and the electrode separation is as small as possible. Because we have not completed and verified a quantitative model for the nonlinear behavior of the device, we hesitate to propose a quantitative limit to the transducer's bandwidth[9]. Using the conservative parameters of Fig. 21 and a series tuning inductor, the absolute impedance of Fig. 22 is obtained. The figure shows a 5% 3 dB bandwidth, which enables the realization of an impressive system. The room temperature thermal noise due to a 50 Ω resistor with 5% bandwidth centered at 10 MHz is 63 nV, or 1.26 nA. The thermal current noise is comparable to that of well-designed electronics, and can be taken as the limiting noise floor of the system. Thus, a transmitter capable of generating 13 mA of current (or for a 50 Ω transmitter, 8 mW of acoustic power all directed at the receiver) will result in a system with 140 dB dynamic range at 10 MHz with 5% bandwidth. Trading some dynamic range for bandwidth yields a system with 120 dB of dynamic range and 50% bandwidth. In short, the extrapolation of the theoretical models herein presented and verified indicates that optimized MUTs may have liquid-coupled performance comparable to piezoelectric transducers' performance.

[9]For example, if the collapse point occurs at electric fields greater than 4.10^8 V/m, a 3 dB bandwidth in excess of 100% is possible.

VII. Conclusion

We have reported that microfabricated ultrasonic transducers are capable of transmitting sound in air with a dynamic range of 110 dB. Such transducers are used to demonstrate air-coupled through transmission in aluminum. MUTs are also shown to work well in water, though their optimized configuration awaits future fabrication runs. Most significantly, we have proposed a theoretical model which agrees with observed behavior. Admittedly, the model only accounts for the electrical impedance behavior of the transducers, which does not completely describe the acoustic behavior of the devices. More direct measurements of the displacements at the transducers' surface and of the directivity of the transducers are planned, and future theoretical models should also describe the observed behavior. The current model nevertheless indicates that MUTs offer better performance than piezoelectric transducers in air-coupled applications, and that MUTs have the potential to approach piezoelectrics' performance in liquids. MUTs enjoy the inherent advantages of microfabrication, which include low cost, array fabrication, and the possibility to integrate electronics either on chip or as a multi-chip module. Additional plans for future work include obtaining a better understanding of the devices' non-linear characteristics when operated at large displacements, the realization of optimized immersion transducers, and the use of the air transducers in several newly enabled applications. More distant plans include array and electronics fabrication and integration.

Acknowledgments

This work was made possible with support from the U.S. Office of Naval Research. X. J. would also like to acknowledge the support of an NUS fellowship. During the course of study, A. A. was with Ginzton Lab, on leave from Bilkent University, Turkey. The staff of the Stanford Nanofabrication Facility, as well as Tom Carver and Pauline Prather of the Ginzton Lab, provided valuable technician support. I. L. also wishes to thank Joseph Mallon for preliminary discussions that resulted in the hexagonal design.

References

[1] S. P. Kelly, R. Farlow, and G. Hayward, "Applications of through-air ultrasound for rapid NDE scanning in the aerospace industry," *IEEE Trans. Ultrason., Ferroelect., Freq. Contr.*, vol. 43, pp. 581–591, July 1996.

[2] A. Gachagan and G. Hayward, "Characterization of air-coupled transducers," *IEEE Trans. Ultrason., Ferroelect., Freq. Contr.*, vol. 43, pp. 678–689, July 1996.

[3] G. Hayward and A. Gachagan, "An evaluation of 1-3 connectivity composite transducers for air-coupled ultrasonic applications," *J. Acoust. Soc. Amer.*, vol. 99, pp. 2148–2157, Apr. 1996.

[4] W. Manthey, N. Kroemer, and V. Magori, "Ultrasonic transducers and transducer arrays for applications in air," *Meas. Sci. Technol.*, vol. 3, pp. 249–261, 1992.

[5] D. W. Schindel and D. A. Hutchins, "Applications of micromachined capacitance transducers in air-coupled ultrasonics and nondestructive evaluation," *IEEE Trans. Ultrason., Ferroelect., Freq. Contr.*, vol. 42, pp. 51–58, Jan. 1995.

[6] J.-yu Lu and J. F. Greenleaf, "A study of two-dimensional array transducers for limited diffraction beams," *IEEE Trans. Ultrason., Ferroelect., Freq. Contr.*, vol. 41, pp. 724–739, Sep. 1994.

[7] R. L. Goldberg and S. W. Smith, "Multilayer piezoelectric ceramics for two-dimensional array transducers," *IEEE Trans. Ultrason., Ferroelect., Freq. Contr.*, vol. 41, pp. 761–771, Sep. 1994.

[8] J. E. Hyslop, J. T. Bennet, and G. Hayward, "An investigation into the design of high frequency two-dimensional arrays for ultrasonic imaging," in *Ultrasonics Symposium*, Cannes, France, 1994, pp. 1515–1518.

[9] G. S. Kino, *Acoustic Waves: Devices, Imaging, and Analog Signal Processing*. Englewood Cliffs, NJ: Prentice-Hall, 1987.

[10] L. F. Degertekin, J. Pei, B. T. Khuri-Yakub, and K. C. Saraswat, "In situ acoustic temperature tomography of semiconductor wafers," *Appl. Phys. Lett.*, vol. 64, pp. 1338–1340, Mar. 1994.

[11] L. F. Degertekin and B. T. Khuri-Yakub, "Hertzian contact transducers for nondestructive evaluation," *J. Acoust. Soc. Amer.*, vol. 99, pp. 299–308, Jan. 1996.

[12] R. M. White, "Generation of elastic waves by transient surface heating," *J. Appl. Phys.*, vol. 34, pp. 3559–3567, 1963.

[13] J. P. Monchalin, J. D. Aussel, R. Heon, C. K. Jen, A. Boudreault, and R. Bernier, "Measurement of in-plane and out-of-plane ultrasonic displacements by optical heterodyne interferometry," *J. Nondestr. Eval.*, vol. 8, pp. 121–133, June 1989.

[14] M.-H. Noroy, D. Royer, and M. Fink, "The laser-generated ultrasonic phased array: analysis and experiments," *J. Acoust. Soc. Amer.*, vol. 94, pp. 1934–1943, Oct. 1993.

[15] W. P. Mason, *Electromechanical Transducers and Wave Filters*. New York: Van Nostrand, 1942.

[16] Z. Skvor, *Vibrating Systems and Their Equivalent Circuits*. Amsterdam: Elsevier, 1991.

[17] W. Khul, G. R. Schodder, and F. K. Schodder, "Condenser transmitters and microphones with solid dielectric for airborne ultrasonics," *Acustica*, vol. 4, pp. 520–532, 1954.

[18] K. Matzuwa, "Capacitive ultrasonic transducer, *J. Phys. Soc. Jpn.*, vol. 13, pp. 1533–1543, 1958.

[19] J. H. Cantrell and J. S. Heyman, "Broadband electrostatic acoustic transducer for ultrasonic measurements in liquids," *Rev. Sci. Instrum.*, vol. 50, pp. 31–33, Jan. 1979.

[20] M. Luukkala and P. Merilainen, "Metal plate testing using airborne ultrasound," *Ultrasonics*, vol. 11, pp. 218–221, Sep. 1973.

[21] W. Grandia and C. M. Fortunko, "NDE applications of air-coupled ultrasonic transducers," in *Ultrasonics Symposium*, Seattle, WA, 1995, pp. 697–709.

[22] D. W. Schindel, "Air-coupled generation and detection of ultrasonic bulk-waves in metals using micromachined capacitance transducers," *Ultrasonics*, vol. 35, pp. 179–181, Mar. 1997.

[23] D. Hohm and G. Hess, "A subminiature condenser microphone with silicon-nitride membrane and silicon backplate," *J. Acoust. Soc. Amer.*, vol. 85, pp. 476–480, Jan. 1989.

[24] M. Rafiq and C. Wykes, "The performance of capacitive ultrasonic transducers using V-grooved backplates," *Meas. Sci. Technol.*, vol. 2, pp. 168–174, Feb. 1991.

[25] M. Pentti, F. Tsuzuki, H. Vaataja, and K. Sasaki, "Electroacoustic model for electrostatic ultrasonic transducers with V-grooved backplates," *IEEE Trans. Ultrason., Ferroelect., Freq. Contr.*, vol. 42, pp. 1–7, Jan. 1995.

[26] D. W. Schindel, D. A. Hutchins, L. Zou, and M. Sayer, "The design and characterization of micromachined air-coupled capacitance transducers," *IEEE Trans. Ultrason., Ferroelect., Freq. Contr.*, vol. 42, pp. 42–50, Jan. 1995.

[27] K. Suzuki, K. Higuchi, and H. Tanigawa, "A silicon electrostatic ultrasonic transducer," *IEEE Trans. Ultrason., Ferroelect., Freq. Contr.*, vol. 36, pp. 620–627, Nov. 1989.

[28] M. J. Anderson, J. A. Hill, C. M. Fortunko, N. S. Dogan, and R. D. Moore, "Broadband electrostatic transducers: Modeling and experiments," *J. Acoust. Soc. Amer.*, vol. 97, pp. 262–272, Jan. 1995.

[29] M. I. Haller and B. T. Khuri-Yakub, "A surface micromachined electrostatic ultrasonic air transducer," in *Ultrasonics Symposium*, Cannes, France, 1994, pp. 1241–1244.

[30] M. I. Haller and B. T. Khuri-Yakub, "A surface micromachined electrostatic ultrasonic air transducer," *IEEE Trans. Ultrason., Ferroelect., Freq. Contr.*, vol. 43, pp. 1–6, Jan. 1996.

[31] M. I. Haller, "Micromachined ultrasonic devices and materials," Ph.D. dissertation, Stanford Univ., Stanford, CA, 1997.

[32] I. Ladabaum, B. T. Khuri-Yakub, D. Spoliansky, and M. I. Haller, "Micromachined ultrasonic transducers MUTs," in *Ultrasonics Symposium*, Seattle, WA, 1995, pp. 501–504.

[33] I. Ladabaum, B. T. Khuri-Yakub, and D. Spoliansky, "Micromachined ultrasonic transducers: 11.4 MHz transmission in air and more," *Appl. Phys. Lett.*, vol. 68, pp. 7–9, Jan. 1996.

[34] H. T. Soh, I. Ladabaum, A. Atalar, C. F. Quate, and B. T. Khuri-Yakub, "Silicon micromachined ultrasonic immersion transducers," *Appl. Phys. Lett.*, vol. 69, pp. 3674–3676, Dec. 1996.

[35] I. Ladabaum, X. C. Jin, H. T. Soh, F. Pierre, A. Atalar, and B. T. Khuri-Yakub, "Micromachined ultrasonic transducers: towards robust models and immersion devices," in *Ultrasonics Symposium*, San Antonio, TX, 1996, pp. 335–338.

[36] X. Jin, I. Ladabaum, and B. T. Khuri-Yakub, "The microfabrication of capacitive ultrasonic transducers," in *Transducers 97*, Chicago, 1997, pp. 437–440.

[37] P. Eccardt, K. Niederer, T. Scheiter, and C. Hierold, "Surface micromachined ultrasound transducers in CMOS technology," in *Ultrasonics Symposium*, San Antonio, TX, 1996, pp. 959–962.

[38] J. W. (Lord Rayleigh) Strutt, *The Theory of Sound*. New York: Macmillan, 1877–78.

[39] L. E. Kinsler, A. R. Frey, A. B. Coppens, and J. V. Sanders, *Fundamentals of Acoustics*. New York: Wiley, 1982.

Igal Ladabaum (S'91) received a B.S. in Bioengineering from U.C. Berkeley in 1992. He then went to Paris, France where he was a Jean Monnet scholar (1992–93) at the Ecole Polytechnique. He was also a staff engineer at Air Liquide. In 1996, he received an M.S. in Electrical Engineering from Stanford University. Currently a doctoral candidate at Stanford, Mr. Ladabaum is interested in the techniques of micromachining and their application to the realization of novel transducers. Most of his effort is directed toward the development and application of ultrasonic transducers. He is a member of the IEEE and the Acoustical Society of America. He has received numerous awards through the course of his studies, including being the student speaker at every commencement ceremony since 8th grade. He received the best student paper prize at the International Conference of Micro and Nano-Engineering in Aix en Provence, France, 1995, and the RWB Stephens Best Student Paper Prize in Ultrasonics International Conference, Delft, the Netherlands, in July 1997. He has contributed several journal and conference papers, and is pursuing patents for some of his work on ultrasonic transducers.

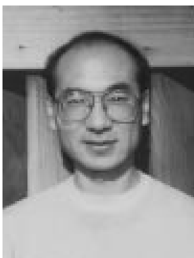

XueCheng Jin (S'93) received the BEng Degree in Biomedical Engineering from Tsinghua University, PR China, in 1990 and the MEng Degree in Computer Engineering from the National University of Singapore, Singapore, in 1994. He is currently studying toward the Ph.D. degree in Electrical Engineering at Stanford University. He worked for Oriental Star Microcomputers, PR China, until 1992, where he designed analog and digital circuits for various instrumentation. He then worked for Texas Instruments Pte Ltd, Singapore, where he designed computer vision algorithms and software codes for real time post mount die inspection in die bonder machines. In 1995, he joined the faculty of Electrical Engineering Department, National University of Singapore, as a Senior Tutor, where he is primarily engaged in research into solid-state sensor and actuator, MEMS and micromachining technology, CMOS integrated circuit design, bioinstrumentation and its miniaturization, medical image processing and computer vision.

XueCheng Jin is a member of IEEE. He serves as a reviewer for several international journals with about 20 publications. He received RWB Stephens Best Student Paper Prize in Ultrasonics International Conference, Delft, the Netherlands, in July 1997 and Whitaker Student Paper Finalist Certificate in IEEE International Conference on Engineering in Medicine and Biology, Baltimore, MD, in November 1994.

Hyongsok T. Soh received a B.S. degree with Distinction in 1992 with a double major in Mechanical Engineering and Materials Science, and an M.Eng degree in 1993 in Electrical Engineering all from Cornell University. He is currently working on the Ph.D. degree in Electrical Engineering at Stanford. His research is on scanning probe lithography and nanometer scale electron devices.

Abdullah Atalar (M'88–SM'90) was born in Gaziantep, Turkey, in 1954. He received a B.S. degree from Middle East Technical University, in 1974; M.S. and Ph.D. degrees from Stanford University in 1976 and 1978, respectively, all in Electrical Engineering. His thesis work was on reflection acoustic microscopy. From 1978 to 1980 he was first a Post Doctoral Fellow and later an Engineering Research Associate in Stanford University continuing his work on acoustic microscopy. For 8 months he was with Hewlett Packard Labs, Palo Alto, engaged in photoacoustics research. From 1980 to 1986 he was on the faculty of the Middle East Technical University as an Assistant Professor. From 1982 to 1983 on leave from University, he was with Ernst Leitz Wetzlar, West Germany, where he was involved in the development of the commercial acoustic microscope. In 1986 he joined the Bilkent University as the chairman of the Electrical and Electronics Engineering Department and served in the founding of the Department where he is now a Professor. He is presently the Provost of Bilkent University. He teaches undergraduate and graduate courses on VLSI design and microwave electronics. His current research interests include micromachined sensors and actuators and computer aided design in Electrical Engineering. He is the project director of a NATO SFS project: TU-MIMIC. He is a senior member of IEEE.

Butrus T. Khuri-Yakub (S'70–S'73–M'76–SM'87–F'95) was born in Beirut, Lebanon. He received the B.S. degree in 1970 from the American University of Beirut, the M.S. degree in 1972 from Dartmouth College, and the Ph.D. degree in 1975 from Stanford University, all in electrical engineering. He joined the research staff at the E. L. Ginzton Laboratory of Stanford University in 1976 as a research associate. He was promoted to a Senior Research Associate in 1978, and to a Professor of Electrical Engineering (Research) in 1982. He has served on many university committees such as graduate admissions, undergraduate academic council of the school of engineering, and others. He has been teaching both at the graduate and undergraduate levels for over 15 years, and his current research interests include in-situ acoustic sensors (temperature, film thickness, resist cure) for monitoring and control of integrated circuits manufacturing processes, micromachining silicon to make acoustic materials and devices such as air borne and water immersion ultrasonic transducers and arrays, and fluid ejectors, and in the field of ultrasonic nondestructive evaluation and acoustic imaging and microscopy.

Professor Khuri-Yakub is a fellow of the IEEE, a senior member of the Acoustical Society of America, and a member of Tau Beta Pi. He is associate editor of Research in Nondestructive Evaluation, a Journal of the American Society for Nondestructive Testing; and a member of the AdCom of the IEEE group on Ultrasonics Ferroelectrics and Frequency Control (1/1/94–1/1/97). He has authored about 300 publications and has been principal inventor or coinventor on over 30 patents. He received the Stanford University School of Engineering Distinguished Advisor Award, June 1987, and the Medal of the City of Bordeaux for contributions to NDE, 1983.